Chapter

Technologies for Deviation of Asteroids and Cleaning of Earth Orbit by Space Debris

Constantin Sandu, Cristian-Teodor Olariu and Radu-Constantin Sandu

Abstract

The present chapter presents the advanced design and technology of special equipment (SECSL) which uses concentrated solar light for deviation of asteroids and cleaning the space of debris. The elliptical orbit of any cosmic body as presented in Einstein's general theory of relativity is rotating around the ellipse center. The trajectory of a cosmic body is permanently affected by the gravity of other moving cosmic bodies. In the case of asteroids (relatively small masses), orbit changes can lead to a collision with the Earth. At this very moment, our civilization has no efficient and reliable mean to destroy or divert a cosmic body heading toward the Earth. This new idea represents a "light canon" which uses concentrated solar light for deviation or vaporization of dangerous asteroids. The equipment is composed out of two parabolic mirrors (one large and one small) with the same focal point and coincident axes. The mirrors reflect the sunlight between them hence the term "concentrated solar light." Next, a similar idea to the SECSL equipment is presented but applied to space debris caused mostly by humans and a new way of disintegrating satellites, spent rocket boosters, thrust chambers, etc. in the Earth's atmosphere during reentry.

Keywords: parabolic mirror, concentrated solar light, equipment, asteroid, satellite, disintegration, cosmic body, deorbit, reentry, space debris, atmosphere

1. Introduction

Today, there is no reliable nor efficient system which can destroy or deflect asteroids or comets on a collision trajectory with the Earth. At this very moment, we cannot comprehend what could happen if an asteroid impacts the Earth. On April 13, 2029, we might experience just that because asteroid Apophis will pass below the orbit of low earth orbit (LEO) satellites and its exact trajectory cannot be predicted.

Albert Einstein, in his general theory of relativity, says that the elliptical orbit of any cosmic body is rotating around the ellipse center (i.e., the perihelion of the orbit is moving continuously). The elliptical orbit or trajectory of any cosmic body (i.e., asteroids, comets, etc.) can be permanently altered by the gravity of other asteroids and planets. Due to this reason, asteroids can be involved in collisions that cause sudden trajectory changes. The trajectory change could one day be toward the

Earth, because asteroids have relatively small masses; thus a change in its trajectory is significant.

According to estimates, there are over 150 million asteroids in our solar system, most of them are grouped in what is called an asteroid belt (see **Figure 1**) and have trajectories passing close to the Earth (see **Figure 2**). NASA's revised estimate of the number of near-Earth asteroids provided by Wide-field Infrared Survey Explorer (WISE) during the NEOWISE project had the number of larger than 100-m objects which are considered medium- to large-sized asteroids at 500. Near-Earth asteroids smaller than 100 m were not studied, and at a later time, near-Earth comets will be analyzed.

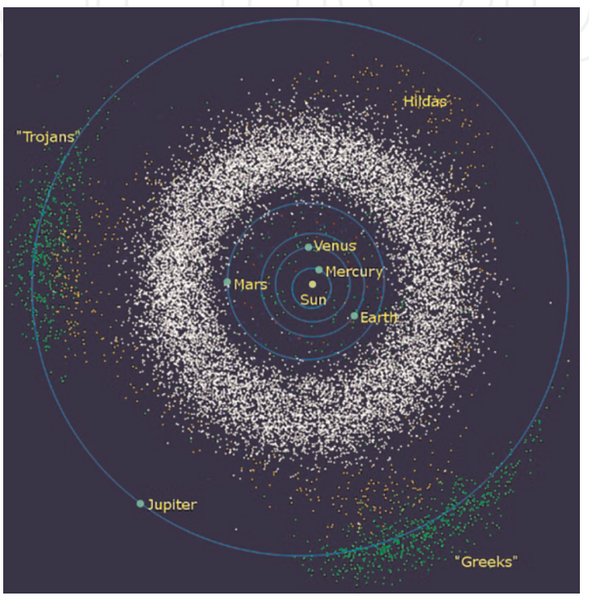

Figure 1.
Asteroid belt.

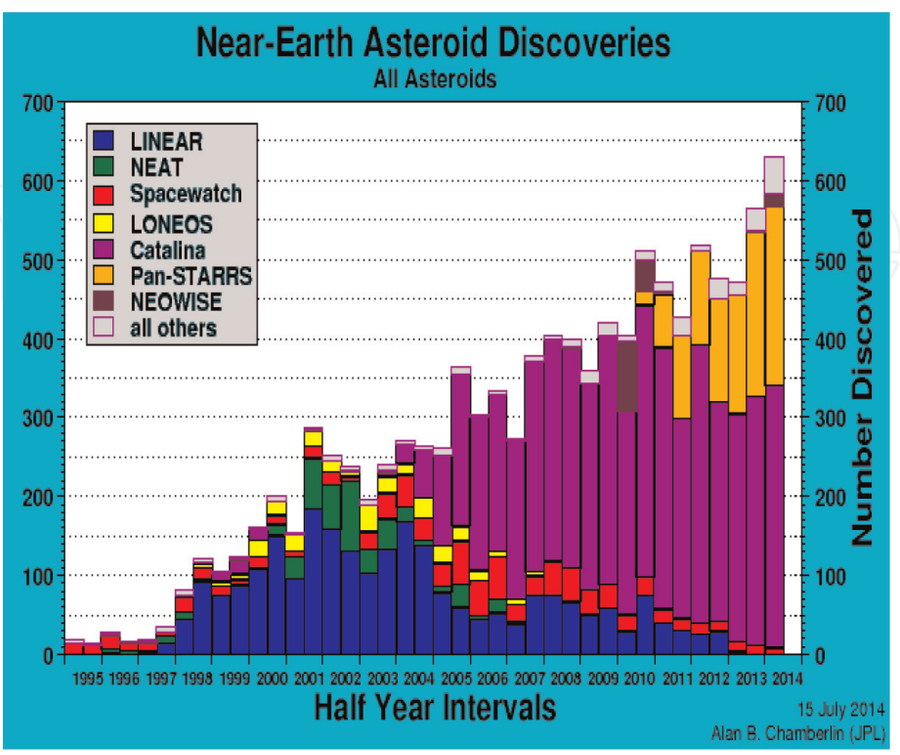

Figure 2.
Near-Earth discovered steroids.

For asteroids larger than 1000 m, the revised number is down to 981 from a prior estimate of about 1000. Out of the 981 large-sized asteroids, NASA managed to estimate with great precision the size of each individual.

The number of asteroids that disintegrate into the atmosphere is surprisingly very high (see **Figure 3**) which demonstrates that the problem with asteroid impact is very alarming.

Two proposed solutions for the Earth's protection against asteroids are synthesized in [1]. The first protection method is presented in **Figure 4**, and it relies on capturing small celestial objects. The second method is presented in **Figure 5**, and it relies on a satellite carrying a nuclear-powered laser which deflects asteroids through local vaporization (laser ablation).

Other solutions propose asteroid gravity tractor, kinetic impact, nuclear explosive devices, etc. It is quite clear that these solutions are not completely satisfactory.

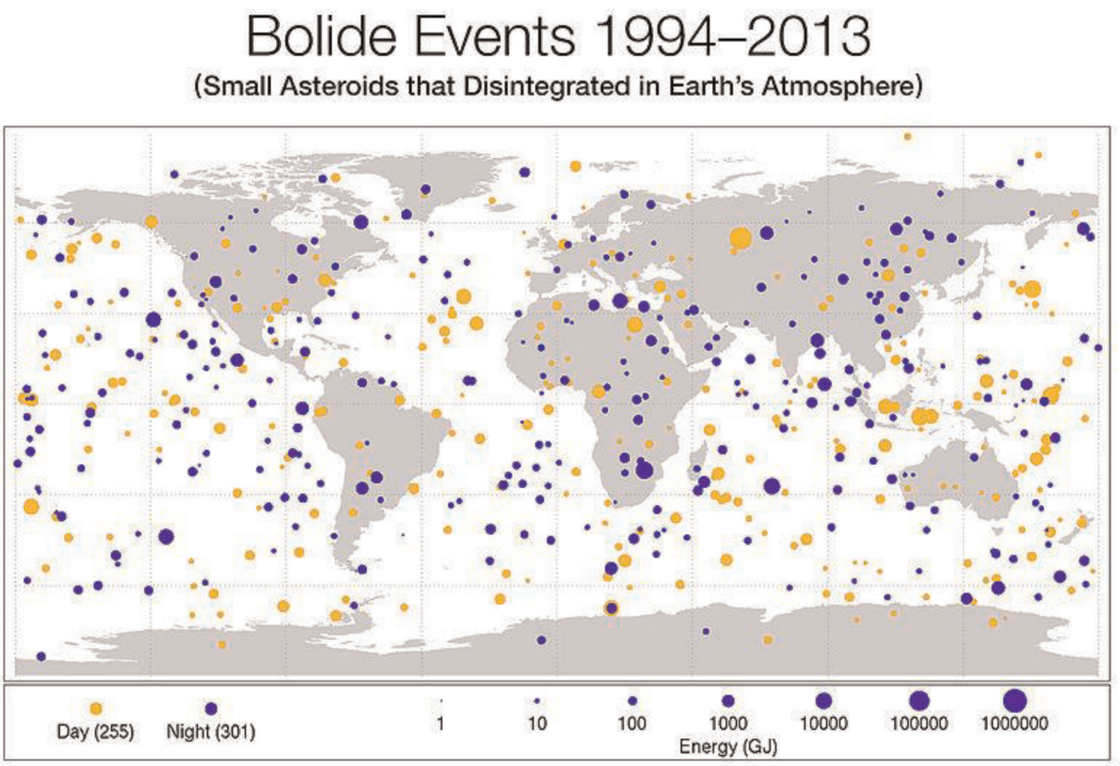

Figure 3.
Number of asteroids that have been disintegrated in the Earth's atmosphere during 1994–2013.

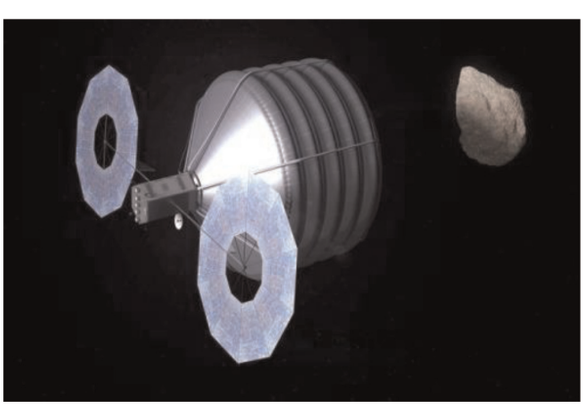

Figure 4.
Asteroid capture system.

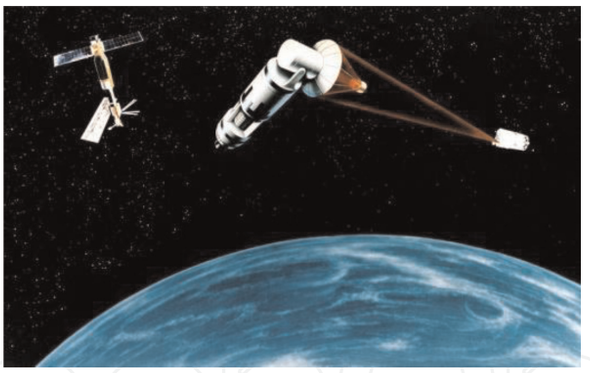

Figure 5.
Asteroid deflection using laser rays.

Asteroids can be very large objects, most of them are rotating conglomerates formed through accumulation of debris after colliding with other asteroids.

Measurements of rotation rates of large asteroids located in the asteroids belt yielded no upper limit. No asteroid with a diameter larger than 100 m has a rotation period smaller than 2.2 h. However, a solid object formed through accumulation of debris after collisions between asteroids should be able to rotate much faster. Due to these issues, the Earth's protection against asteroids has no satisfactory solution just yet.

Also in the near-Earth region, there are not only asteroids and comets, there's also man-made debris as a result of space exploration missions manned and unmanned. Man-made space debris already represents a great threat to the safety of space exploration and exploitation. Most of the space debris is concentrated in the near-Earth space region in the low earth orbit (LEO) and geostationary earth orbit (GEO) (see **Figures 6** and 7). Space debris are composed of nonfunctional rocket boosters, spent rocket upper stages, paint flakes, chunks of slag from solid rocket motors, old science experiment equipment, nonfunctional satellites, various fragments which are the result of collisions, satellite components destroyed by missiles, and materials detached from the International Space Station (ISS) [4].

Just like asteroids, space debris can be classified by their dimensions:

- Category I: size <1 cm—can cause significant damage to vulnerable parts of the satellite.
- Category II: size 1 to 10 cm—can cause serious damage to or destroy a satellite; there is no effective shielding against this category of debris.
- Category III: size >10 cm—can destroy a satellite by collision; it can be tracked, and the satellite can perform evasive maneuvers to avoid collision.

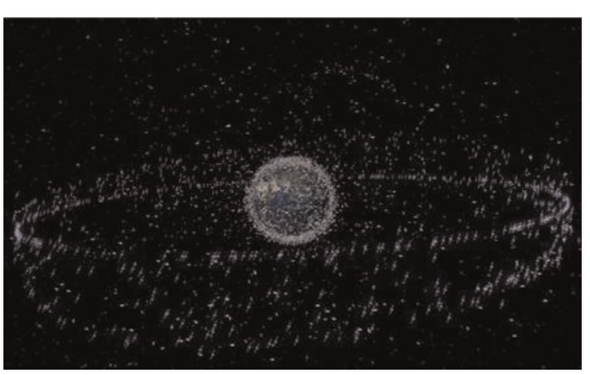

Figure 6.
Space debris in the LEO region [2].

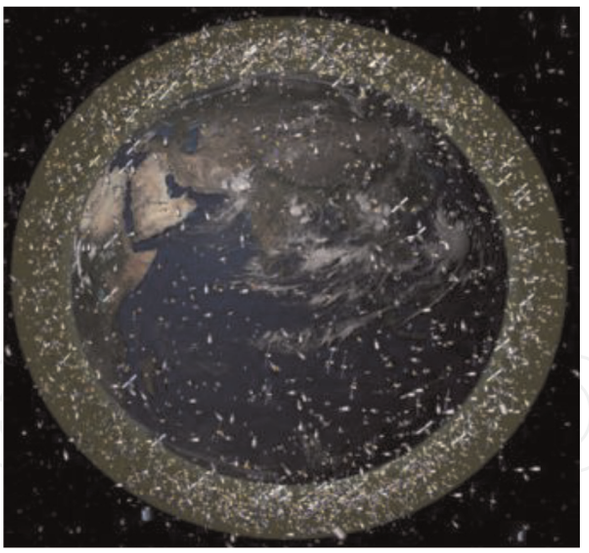

Figure 7.
Space debris in the GEO region [3].

Today, the growth of space activities is exponential, but this growth has generated an important problem: the need for rapid disintegration of space debris after reentry in the Earth's atmosphere. Space debris as stated earlier represents nonfunctional man-made objects or fragments of such objects. Only 6% of catalogued objects are functional, the rest of them are space debris [3]. At the end of their operational life, satellites reenter the Earth's atmosphere being disintegrated through burning initiated by the friction with air. This is happening for the final rocket stages which become space debris after the propellant has been depleted. In many cases the space debris fallen on the ground had large dimensions (helium tanks, thrust chambers, propellant tank, pressure sphere) [5].

The lifetime of a man-made object is very long; for example, satellites of the Satellite Pour l'Observation de la Terre or Satellite for Observation of Earth (SPOT) family placed on a Sun-synchronous orbit can orbit for about 200 years at 822 km altitude representing a high risk for other satellites [6]. Regulations were issued for direct deorbiting of satellites after finishing their operational life, but these regulations do not solve the need for rapid burning of satellites in the atmosphere; thus big chunks of unburned metal could fall on the ground [7].

The European Space Agency (ESA) came with a proposal to solve this problem under the name of "Design for Demise," according to which space equipment design must take into account the on-ground safety requirements [8].

The "Design for Demise" proposes that separation of satellite into components due to the centrifugal forces should be done during the reentry procedure. Although this is a good idea, it still does not respond to the need of rapid burning in the atmosphere, and again big chunks of unburned metal could fall on the ground.

For each of the upper-mentioned problems, there is a potential solution in the form of a system or a new way of designing space equipment. In the next chapter, each system will be presented in detail.

2. Special equipment which uses concentrated solar light for earth protection against asteroids: "light gun"

The special equipment which uses concentrated solar light for Earth protection against asteroids proposed in this paper could be placed on a solar orbit close to the Earth or on the Earth's orbit. This special equipment represents a system which

includes one large and one small parabolic mirrors both highly reflective and with the same focal point. The reflectivity of a mirror is given by reflective foils (or plates) which are stretched on a lightweight parabolic support for the mirror. The light rays coming from the Sun are focalized by the large parabolic mirror onto the focal point; afterward they are reflected by the small parabolic mirror as a group of parallel rays which pass through a central hole located in the center of the large parabolic mirror. A mirror tube attached to the large parabolic mirror by means of an articulation permits the orientation of the concentrated light beam as required (see **Figure 8**).

The role and functions of the main components:

1. Large parabolic mirror. Role: capture and focus sunlight onto the common focal point.

2. Small parabolic mirror. Role: receives the light rays coming from the large parabolic mirror and reflects them forming a beam of concentrated parallel rays of light.

3. Mobile mirror tube guide. Role: directs the light beam as required.

4. Spherical articulation. Role: permits the rotation of the light guide around one point.

5. Resistance structure. Role: keeps in position the foil forming the large parabolic structure. The foil is stretched on this structure.

6. Connection structure. Role: aligns the mirrors so their axes are always parallel and their focal point is common.

7. Positioning engines. Role: keep the SECSL in the correct position and maintain stability.

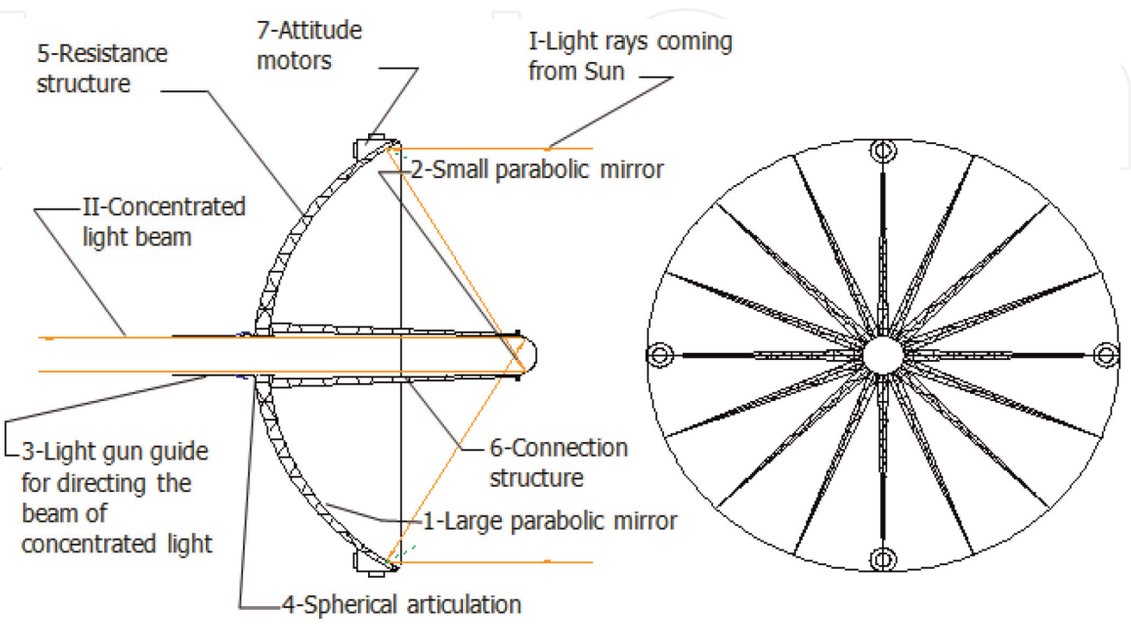

Figure 8.
Main design features of SECSL.

The SECSL is table in space; according to the law of momentum conservation, the sum of all light impulses is zero. However, when the light beam is directed toward the target, this balance is changed, and compensation forces must be applied to keep the system in position (i.e., with the concave side of the large parabolic mirror oriented toward the Sun).

2.1 Estimating the power of a SECSL system

Solar power is the key future for our civilization to expand in space. The main component of this power is electromagnetic radiation. The spectrum of solar radiation is the spectrum of a black body having a temperature of 5800 K [9]. The electromagnetic radiation is emitted in a broadband of frequencies. Electromagnetic energy is initially emitted in the range of gamma rays, as a result of nuclear fusion reactions. Gamma rays during their travel from the Sun's core to the surface are converted into low-energy photons. Thus the Sun does not emit gamma rays; it emits only X-rays, ultraviolet light, visible light, infrared light, and radio waves. The spectrum of nearly all solar electromagnetic radiation striking the Earth's atmosphere ranges from 100 nm to 1 mm.

In **Figure 9** the power emitted by the Sun under the form of X rays and ultraviolet is low. Most of the power is emitted in the range of visible light. Infrared and radio frequencies have less power. Assuming the SECSL is placed near the Earth, the irradiance can be assumed to be $E_e = 1360\ W/m^2$.

Both mirrors are made from gold-plated Mylar foil with remarkable reflectivity coefficient [10]. **Figure 10** shows that for most frequencies, gold has a reflection coefficient of $R_g = 0.98$ compared to aluminium or silver. In the case of the SECSL, the best foil should be made of gold-plated fine and thin graphite fabric due to gold's remarkable reflection coefficient and graphite's high heat transfer coefficient and high emissivity coefficient.

If the large parabolic mirror is oriented with the reflective (concave) face towards the Sun, the amount of energy captured is maximized.

For example, if the large mirror has a radius of r = 10 m and assuming the solar irradiance is $E_e = 1360\ W/m^2$, the total collected power is

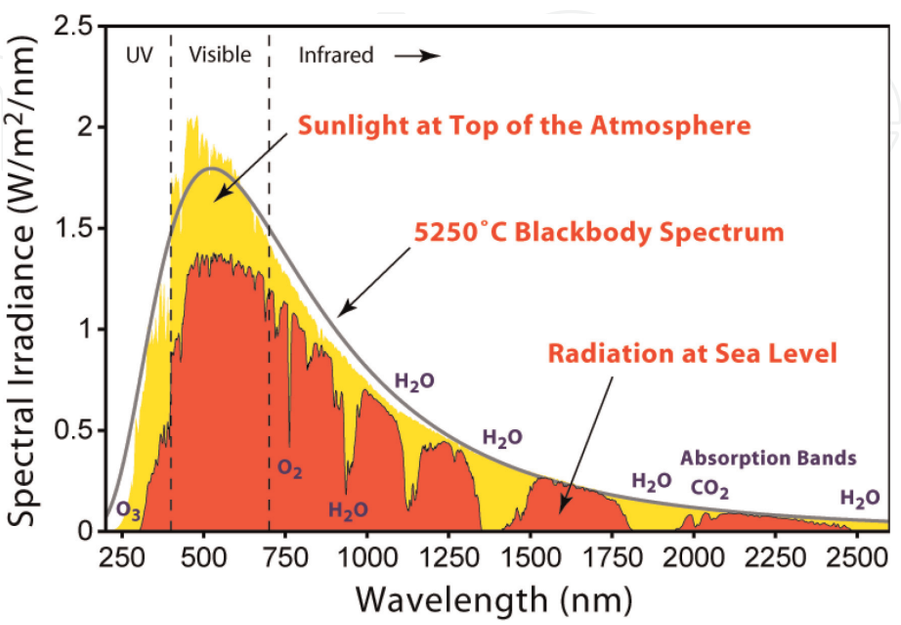

Figure 9.
The spectrum of the Sun.

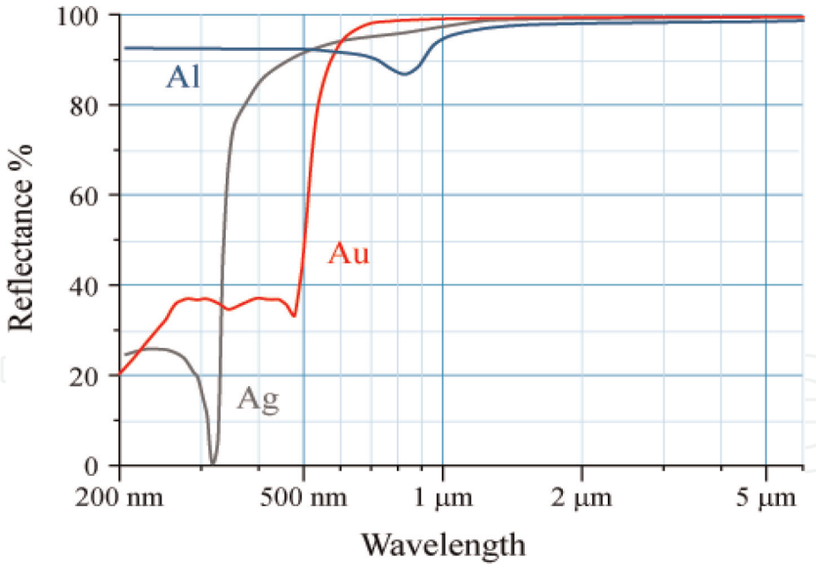

Figure 10.
Reflection coefficient of metals.

$$P = E_e \cdot \pi \cdot r^2 = 1360 \cdot \pi \cdot 10^2 = 427.256\ \text{kW} \quad (1)$$

The total collected power is significant. However, when this radius increases, the power collected from the Sun becomes very high. **Table 1** shows the correlation between the SECSL mirror diameter and the amount of collected power. As shown in the table, when the radius of the large parabolic mirror r = 50 m, the collected power is P = 10681.4 kW. Such a mirror is relatively easy to be built in space due to the absence of gravitational forces.

For a simple sample calculation, assume that a SECSL having a radius of large parabolic mirror, r = 50 m, is focused on an iron asteroid for 10 s. Consider iron properties listed in the literature [11]:

Crt. no.	Radius of large parabolic mirror, r (m)	Collected solar power, P (kW)	Crt. no.	Radius of large parabolic mirror, r (km)	Collected solar power, P (terawatt)
1	5	106.8	13	1	0.004
2	10	427.3	14	2	0.017
3	15	961.3	15	3	0.038
4	20	1709.0	16	4	0.068
5	30	3845.3	17	6	0.154
6	40	6836.1	18	8	0.273
7	50	10681.4	19	10	0.427
8	60	15381.2	20	12	0.615
9	70	20935.6	21	14	0.837
10	80	27344.4	22	16	1.093
11	90	34607.8	23	18	1.383
12	100	42725.7	24	20	1.708

Table 1.
Collected solar power for different large parabolic mirror radii.

- Melting temperature: t_m = 1538°C, T_m = 1811 K
- Boiling temperature: t_b = 2862°C, T_b = 3135 K
- Heat capacity: c = 0.45 kJ/kgK (considered the same for solid and liquid iron)
- Heat of fusion: c_f = 247.3 kJ/kg
- Heat of vaporization: c_v = 6088.3 kJ/kg

The heat quantity needed in order to vaporize 1 kg of iron can be calculated:

$$E_1 = 1 \cdot c \cdot (T_b - T_c) + c_f \cdot 1 + c_v \cdot 1 = 0.45 \cdot 3135 + 247.3 + 6088.3 = 7746 \text{ kJ/kg} \quad (2)$$

Reading from **Table 1** the power for the mirror with a radius r = 50 m, in 10 s the power beam into the asteroid is

$$E = 10 \cdot 10681.4 = 106814 \text{ kJ} \quad (3)$$

This total energy can vaporize a mass of iron given by

$$M = \frac{E}{E_1} = \frac{106814}{7746} = 14 \text{ kg} \quad (4)$$

Hitting the asteroid continuously (hundreds or thousands of times) in this manner, it can be deflected from a collision trajectory with the Earth. Even the trajectory of massive asteroids can be changed. Due to local vaporization of the asteroids, mass leads to the apparition of a reaction force produced by the expanding vapors.

In space the construction of such a gigantic system should be easier due to the absence of gravity. Calculations done using the above equations show that an SECSL having the radius of the large parabolic mirror r = 10 km can send a beam of concentrated light into the asteroid at a power of 0.427 terawatt. Such a power can vaporize an iron asteroid having the mass of 100 tons in just 8 s.

The time required to destroy or deflect an asteroid using the SECSL system is reasonably low. Practically, the asteroid can be destroyed in a few minutes because obviously the SECSL beam hits the target with the speed of light.

2.2 Heat transfer calculations

Simple calculations show that SECSL works properly both near the Earth (where irradiance Ee = 1360 W/m^2) and at 0.1 AU distance from the Sun (where irradiance is Es = 136,000 W/m^2).

Assume that a SECSL placed near the Earth having the large parabolic mirror radius r_{LPM} = 10 km and the radius of the small parabolic mirror r_{SPM} = 1.25 km; this system is capable of concentrating the sunlight by a factor of 64.

Consider that the reflection coefficient for a gold-plated foil $R_{gf/p}$ = 0.98 and the emissivity of carbon fabric/plate $e_c \approx 1$.

Assume that the whole power absorbed by the gold-plated foil is radiated according to Stefan-Boltzmann law:

$$E_e \cdot \left(1 - R_{gf/p}\right) \cdot R_{gf/p} \cdot \left(\frac{r_{LPM}}{r_{SPM}}\right)^2 = \sigma \cdot T^4 \quad (5)$$

In Eq. (1) $\sigma = 5.67 \cdot 10^{-8}$ W/m^{2}K^4 represents the Stefan-Boltzmann coefficient for black body radiation. Using the given data, thermal balance is achieved at T = 410 K (t = 137°C), which is under the maximum allowable working temperature for carbon composites with polymeric matrix (t = 280–300°C).

Considering that the thickness of the gold-plated foil is δ = 0.05 mm and the average thermal transfer coefficient for graphite is λ = 80 W/m K at t = 137°C, the temperature difference Δt needed for heat transfer from the gold reflective face to the rear carbon face is given by the following thermal balance equation:

$$E_e \cdot (1 - R_{gf/p}) \cdot R_{gf/p} \cdot \left(\frac{r_{LPM}}{r_{SPM}}\right)^2 = \lambda \cdot \frac{\Delta t}{\delta} \tag{6}$$

For the given equation, the thermal difference necessary for heat transfer would be Δt = 0.001°C; the result shows that heat is quickly transferred from the gold-plated face to the graphite fabric/plate due to the high thermal conductivity of the graphite and small thickness.

At the beginning of this chapter, we've stated that SECSL works properly even at 0.1 AU from the Sun, where the irradiance is 100 times stronger. Considering the same constants and mirror dimensions as before and using Eq. (1) we find that the surface temperature of the small parabolic mirror is T_{SPM} = 1296 K (t_{SPM}=1023°C) which is under the melting point of pure gold (1064°C).

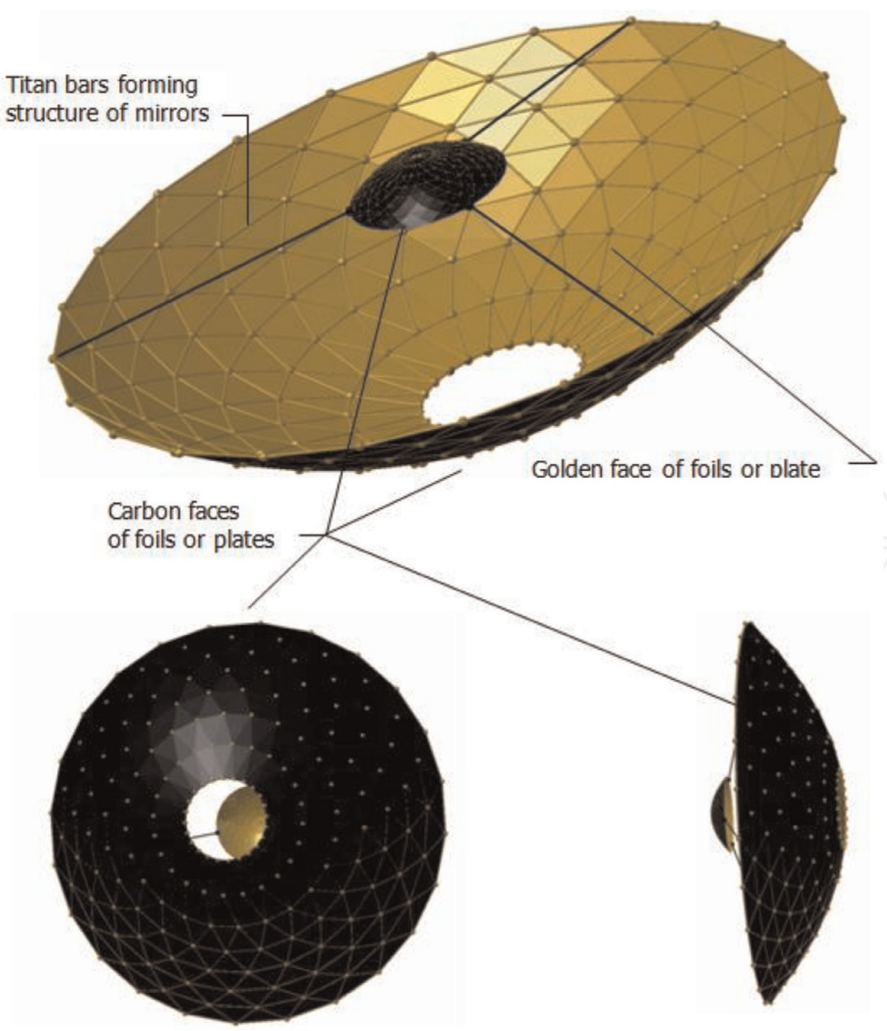

Figure 11.
SECSL equipment built using triangular cells.

Thermal balance at the surface of the large parabolic mirror is achieved at T_{LPM} = 476 K (t_{LPM} = 203°C) still under 280–300°C—the working temperature limit for carbon fiber composite with polymeric matrix.

2.3 SECSL mass calculation

In **Figure 11** the cell design is based on triangular shapes. It can be either hexagonal or rectangular cells, i.e., if rectangular cells are used, it yields a light structure, but the stability is reduced compared to the design of triangular cells. When using gold-plated foils, the structure bars can be square and straight. If gold-plated plates are used, the bars must be curved according to the parabolic surfaces of the mirrors which in this case results in a higher accuracy in focusing the light.

Such a construction can be relatively easily built in space if "SpiderFab" robots are used (see **Figure 12**) [12]. Preliminary calculations show that the resistance structure of the large parabolic mirror can be built from 528 bars with 9.3 m in length. If the bars are square tubes made from titanium having dimensions of $20 \times 20 \times 0.2$ mm^3, calculations show that the total mass is 357 kg. If graphite fiber composites are used instead of titanium, the mass of the large parabolic mirror decreases to about one-third due to the extremely low density of these materials.

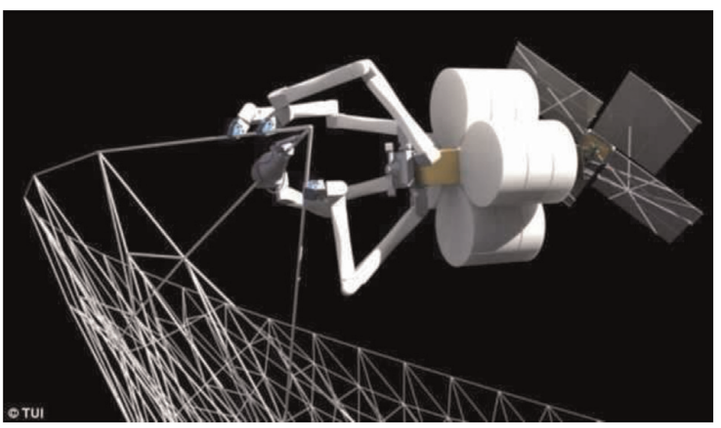

Figure 12.
NASA's SpiderFab robot in space.

3. Solar-thermal system for deorbiting space debris

This system is similar to the one presented in Chapter 2, composed of two parabolic mirrors, a large one and a small one (see **Figure 13**). Just like in the case of SECSL, the mirrors are made from very thin composite material (graphite fiber) plated with gold foils or gold plates on the concave face. The concave faces of the two mirrors face each other having the same focal point. The solar light rays which are parallel to the axis of the large parabolic mirror are reflected into its focal point and onto the small parabolic mirror and form parallel rays which are directed along the common axis. The diameter of the concentrated light beam is the same as the diameter of the small mirror ("d"). The concentrated light beam passes through a cutout (hole) in the center of the large parabolic mirror with diameter d^+. The hole in the large parabolic mirror is closed by a gold-plated shutter.

The system operates as follows: the system is oriented with the large parabolic mirror to the Sun using the attitude thrusters, while the shutter is closed. The light guide tube is aligned with the space debris, and the faces of the lens are curved at the appropriate radii in order to focus the light on the space debris.

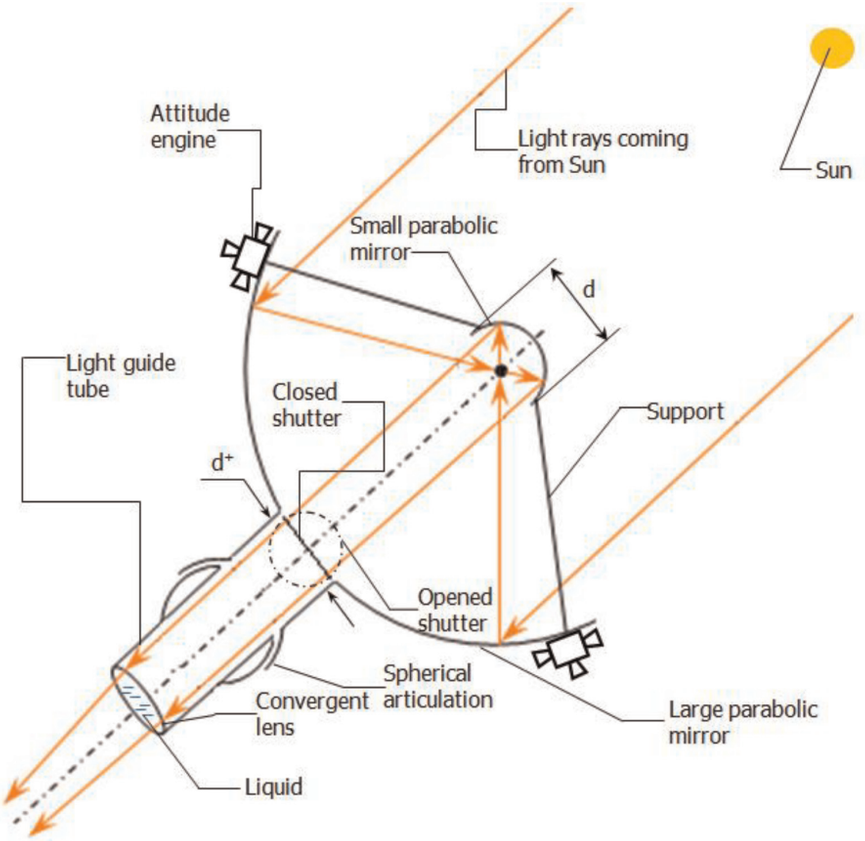

Figure 13.
Design of solar-thermal system.

When the shutter opens, the light coming from the Sun is focused by the large parabolic mirror in the common focal point and then is reflected by the small parabolic mirror toward the hole "d^+" and the light guide tube. At the end of the light tube, the light is focused by the lens in a focal point which is positioned onto the space debris. The focused light locally vaporizes/ionizes the space debris material. The thrust force created pushes the space debris toward the Earth surface where it burns in the atmosphere.

When the shutter is closed, the light rays are sent back toward the small parabolic mirror and back to the Sun.

An alternative to the parabolic mirror system is the Cassegrain-type or Gregorian-type solar-thermal system. These systems are used in manufacturing optical telescopes or radio antennas [13].

Basically, a Cassegrain reflector (see **Figure 14**) [14] is a combination of a large concave and a small convex (hyperbolic) mirror. This design permits placing a focal point at a convenient location behind the large parabolic mirror using a compact mechanical system.

On the other hand, the Gregorian reflector [15] uses a small concave (parabolic) mirror with a focal point that doesn't coincide with the focal point of the large parabolic mirror (see **Figure 14**).

Although the Cassegrain-type and the Gregorian-type solar-thermal system can focus the light in a single point placed behind the large parabolic mirror, it is more difficult to change the focal point distance and direct the concentrated light beam onto the space debris.

3.1 Orbits for the solar-thermal system for space debris deorbiting

This system can be placed on a geocentric orbit, heliocentric orbit, or Sun-synchronous orbit. The most advantageous is the Sun-synchronous orbit (helio-

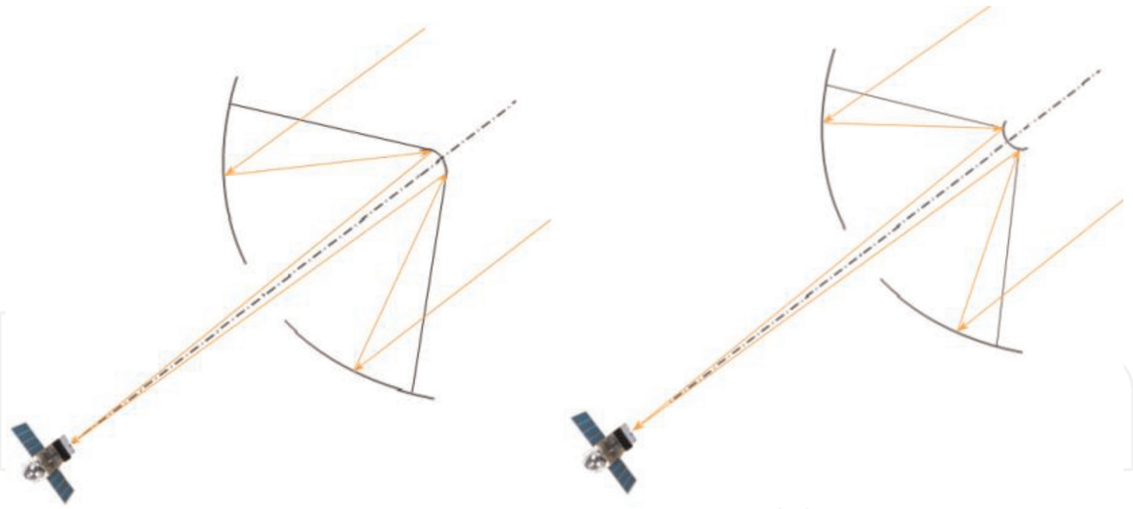

Figure 14.
Gregorian-type (left) and Cassegrain-type (right) solar-thermal systems.

synchronous orbit) [16] because the satellite is placed in constant sunlight. For example, heavy military or weather satellites are placed on Sun-synchronous orbits.

3.2 Lens design

The lens that is placed in the light tube has the role to focus the light on a very small area in order to assure very high power density. Theoretically, the energy can be focused on a geometric point. In reality due to chromatic aberration and shape errors, light is not focused quite precisely. The lens presented in **Figure 15** is made out of and elastic material filled with a colourless liquid.

Approximating surfaces "S1" and "S2" with spheres having radii "r_1" and "r_2," respectively, assuming the thickness of the lends is denoted as "d" and neglecting the optical effect of transparent elastic material (which is very thin) if the refractive index of the liquid is "n," the focal distance "f" of the lens is given by the following equation [13]:

$$\frac{1}{f} = (n-1)\cdot\left[\frac{1}{r_1} - \frac{1}{r_2} + \frac{(n-1)\cdot d}{n\cdot r_1\cdot r_2}\right] \tag{7}$$

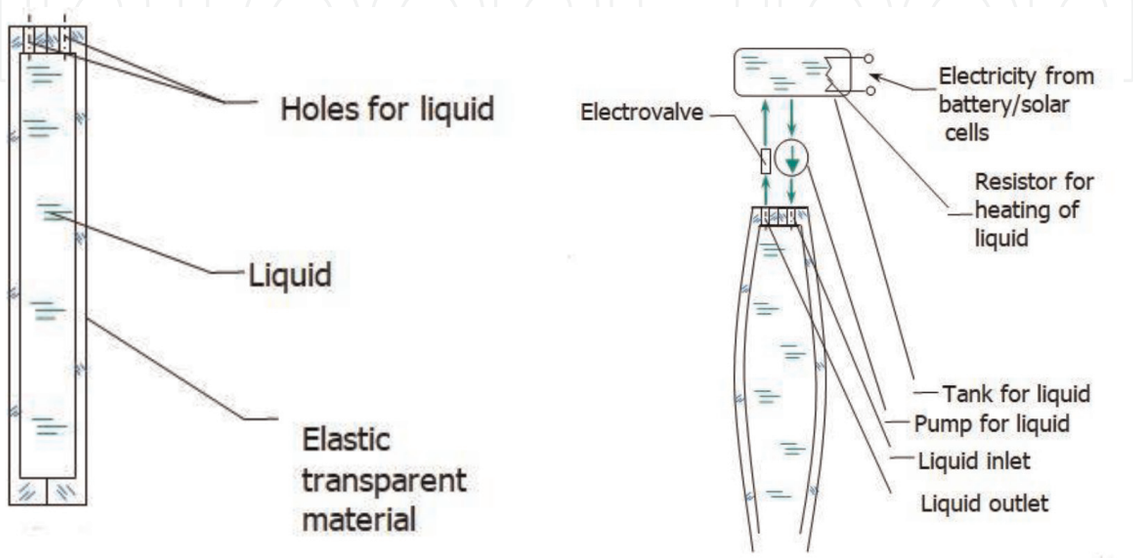

Figure 15.
Lens design filled with liquid.

In order to simplify the case of such model, consider $r_1 = r_2 = r$:

$$\frac{1}{f} = (n-1)\cdot\left[\frac{1}{r} - \frac{1}{r} + \frac{(n-1)\cdot d}{n\cdot r\cdot r}\right] = \frac{(n-1)^2\cdot d}{n\cdot r^2} \tag{8}$$

Eq. (8) shows that for a given n and d, when $r \rightarrow \infty$ (i.e., low pressure of liquid inside the lens), $f \rightarrow \infty$, i.e., theoretically the system can hit the target (space debris) at any distance. However, due to aberration and imprecision of lens dimensions, this distance is limited. Lens operation is illustrated in **Figure 16**.

The temperature of liquid must be kept in an appropriate range for preserving the liquid state (avoiding of freezing). A resistor fed by battery charged by solar cells heats the liquid which is circulated permanently by a pump with a low speed. The electro-valve is normally opened. When hitting the space debris is necessary, the electro-valve is closed, and the liquid bends the lens to the necessary curvature. Some suitable liquids and reflective indexes are given in **Table 2** [17].

The transparent elastic material can be polydimethylsiloxane (PDMS) which has good optical properties and large elongation and is highly transparent (over 96%) in the range of visible wavelengths. PDMS refractive index is $n_{PDMS} = 1.41$. In a terrestrial application, such an elastomeric membrane having 60 microns in thickness was used in manufacturing convex lenses [18]. The refractive liquid used in that design was water.

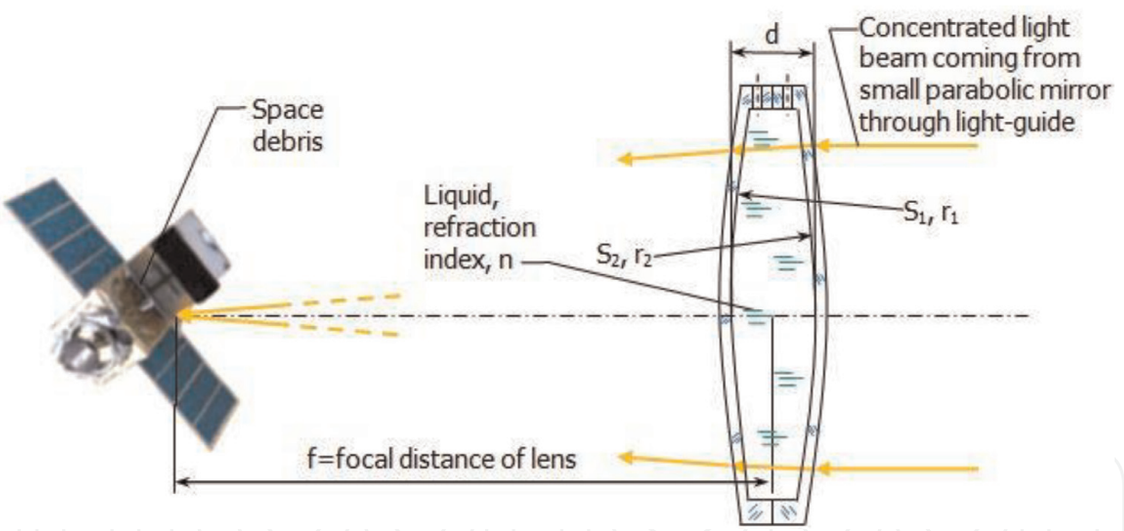

Figure 16.
How a lens filled with liquid operates to eliminate space debris.

No.	Liquid	Refractive index, n
1	Aniline	1.586
2	Benzyl benzoate	1.568
3	Ethylene glycol	1.43
4	Glycerin (glycerol)	1.47
5	Water	1.333

Table 2.
Suitable liquids for lens.

3.3 Estimated power, specific impulse, and thrust calculations

3.3.1 Estimated power calculations

The space debris is made of various metals (aluminium, titanium, carbon fiber composite, steel, etc.). For example, consider a space debris made out of aluminium. In Chapter 2 we've considered the space debris made out of iron.

Consider aluminium properties listed in the literature [19]. For simplicity they are considered constant for a wide range of temperatures:

- Melting temperature: t_m = 660.3°C, T_m = 933.3 K
- Boiling temperature: t_b = 2470°C, T_b = 2743 K
- Heat capacity (solid aluminium): c_S = 0.9 kJ/kg K
- Heat capacity (liquid aluminium): c_L = 1.18 kJ/kg K
- Heat of fusion: c_f = 398 kJ/kg (10.71 kJ/mol)
- Heat of vaporization: c_v = 6088.3 kJ/kg
- First ionization energy: c_{ion} = 577.5 kJ/mol (21,388 kJ/kg)

Using Eq. (2) for 1 kg of aluminium and assuming that the starting temperature T_0 = 0 K, the total heat needed to vaporize aluminium is

$$E_{vap} = 1 \cdot c_S \cdot (T_b - T_0) + c_f \cdot 1 + c_L \cdot (T_b - T_m) + c_v \cdot 1 \tag{9}$$

Making the appropriate substitutions in Eq. (9) results

$$E_{vap} = 0.9 \cdot 2743 + 398 + 1.18 \cdot (2743 - 933.3) + 10518 = 15520 \text{ kJ/kg} \tag{10}$$

The total energy needed to ionize aluminium atoms after vaporization is

$$E_{ion} = E_{vap} + c_{ion} = 15520 + 21388 = 36908 \text{ kJ/kg}$$

In **Table 3** the amount of aluminium that the system can vaporize and ionize in 1 s is presented.

3.3.2 Estimated specific impulse and thrust calculations

The process of generating reaction force due to material ablation is very complex. This effect was observed by pointing a laser to a material surface [20]. In this present case, the process should be similar.

In the case of laser rays, ablation takes place when the material is removed from a substrate through direct absorption of laser ray energy. As a first condition, the radiation energy must exceed a given threshold, which is less than 10 J/cm^2 for metals, 2 J/cm^2 for insulating inorganic materials, and 1 J/cm^2 for organic insulation materials [20].

The solar-thermal system discussed here (see **Table 2**, case no. 1) satisfies this requirement because, even when the power of the smallest mirror is $0.98 \times 0.98 \times 88.4$ = 84.9 kW, it provides an energy of 10 J in 1.18×10^{-4} s [20].

Case no.	Radius of large parabolic mirror, r_{lpm} (m)	Collected solar power, P (kW)	Flow of aluminium vapors per second, g	Flow of aluminium ions (first level) per second, g
1	5	88.4	6	2
2	7.5	240.3	15	7
3	10	427.3	28	12
4	15	961.3	62	26
5	20	1709.0	110	46
6	25	2670.3	172	72

Table 3.
The quantity of aluminium vaporized by the system in 1 s.

Another condition is related to the energy absorption mechanism. Chemical composition, microstructure, and morphology of material strongly influence the absorption of heat.

Heating debris must be sufficiently fast for homogenous nucleation and expansion of vapor bubbles and ions.

Some simulations done for interaction of laser rays have shown that [21]:

- The degree of light absorption increases as the cavity deepens.
- Maximum energy absorbed by the cavity is around 80% of the total energy of radiation.
- The radiation is multiple times reflected by the cavity, and as a result, the energy is highly concentrated at the center and the bottom of the cavity and forms the final conical shape of the cavity.
- The surface temperature is much higher than the normal boiling point.
- In order to be able to remove the material, it must have a homogenous boiling regime and evaporation; the power intensity must be over 108 W/cm^2.

Note: The mentioned simulations have been conducted only for iron, not for aluminium or other materials currently used in manufacturing satellites and space equipment, but the effect should be similar (**Figure 17**).

In some experiments a specific impulse of around 4000 s was measured for carbon and aluminium in ionized state produced by the laser ray [23]:

During those experiments the following observations were made:

- The speed of the ejected atoms and implicitly Isp is inversely proportional to the square roots of the atomic mass of ablated material; the lighter the element the higher the specific impulse.
- Thrust tends to increase with atomic mass of ablated material.
- The speed of the ejected atoms was independent of angle at 22 cm away from the target.
- The ablation time was 1.5 s.

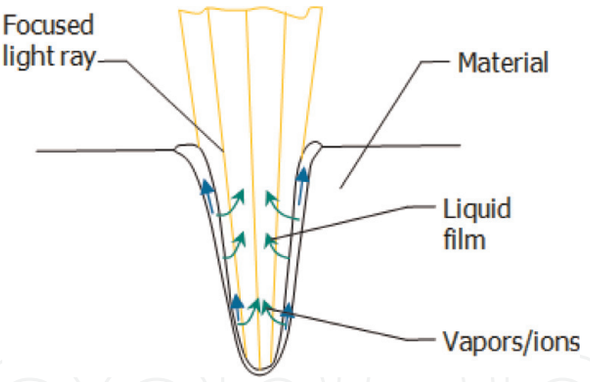

Figure 17.
The effect of a focused light ray on a material [22].

For the case where Isp has a known value, one can evaluate the thrust force by the following equation:

$$T_f = g_0 \cdot I_{sp} \cdot \dot{m} \tag{11}$$

where g_0 represents the gravitational acceleration at the Earth's surface (g_0 = 9.81 m/s^2). $\dot{m}$ represents the mass of ions ejected in 1 s.

Momentum coupling coefficient C_m is another method for thrust evaluation [20]. This coefficient characterizes thrust production efficiency. The coefficient is determined as the thrust to laser power ratio. This parameter determines the minimum light power required to produce a 1 N thrust:

$$C_m = \frac{T_f}{P} \tag{12}$$

According to the above reference, $C_{m\ max}$ Al = 6·10−5 N/W for aluminium. That means that in the case of ablation of a space debris made of aluminium using a solar-thermal system with a power of P = 88.4 kW, the thrust force resulted is

$$T_f = P \cdot C_{m\ max\ Al} = 88400 \cdot 6 \cdot 10^{-5} = 5.3\ N \tag{13}$$

In case the large parabolic mirror has a diameter of r_{lpm} = 25 m, the thrust force is

$$T_{f\ 25} = P \cdot C_{m\ max\ Al} = 2670300 \cdot 6 \cdot 10^{-5} = 160.2\ N \tag{14}$$

In both cases the thrust force is remarkably high and can deorbit space debris with just a few hits.

4. A new design of space equipment for rapid disintegration in atmosphere after reentry

This new design is inspired by the tragic loss of the Space Shuttle Columbia's crew on February 1, 2003 [24]. Columbia disintegrated over Texas and Louisiana when it reentered the Earth's atmosphere. During the launch of the space shuttle, a piece of foam insulation struck the left wing of the orbiter deteriorating its ablative protection [24]. When time came for the space shuttle to reenter the Earth's atmosphere, the damage caused by the foam insulation allowed hot air to penetrate into

the wing creating an irregular hole. Air entered the left wing with high speed, quickly became very hot when stagnating, and destroyed the internal structure of the wing.

4.1 Lessons learned after the Space Shuttle Columbia disaster

During the reentry phase, shock waves produced by hypersonic velocities and the frictional effect of the atmosphere began to heat Columbia's surface. The temperature varied depending on location: the orbiter's nose and leading edges of the wing experiencing temperatures greater than 1538°C [25].

The breach created during launch in the ablative protection of the left wing allowed for hot gases to penetrate the wing and to advance in the same direction inside the wing and to the fuselage (see **Figure 18**). This phase became known as "phase I" from "Initialization."

During the "Initialization" phase, the wing lost its aerodynamic characteristics, and the destruction process was extremely short, lasting from 13:59:37.5 GMT to 13:59:39.7 GMT (2.2 s) (see **Figure 19**) [25].

The "Acceleration" phase quickly followed the "phase I" which lasted for 0.07 s. The destruction continued with total dispersal of the space vehicle and burning in the atmosphere (see **Figure 20**). This phase can be called "phase D" from "Dispersal" and lasted for 55 s (**Figure 21**).

4.2 Space equipment for rapid disintegration during atmosphere reentry

As presented in Chapter 1, ESA's "Design for Demise" concept must be implemented in every space equipment. Following those guidelines, the present paper presents a new vision of that concept.

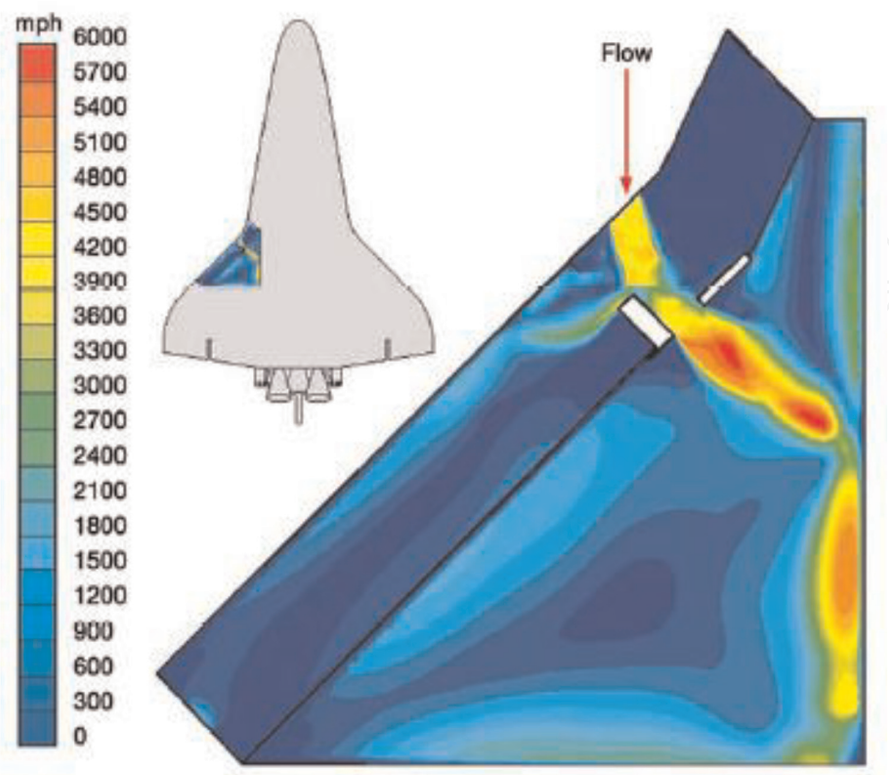

Figure 18.
Velocity distribution on Columbia's left wing at the beginning of the disaster (phase I) [25].

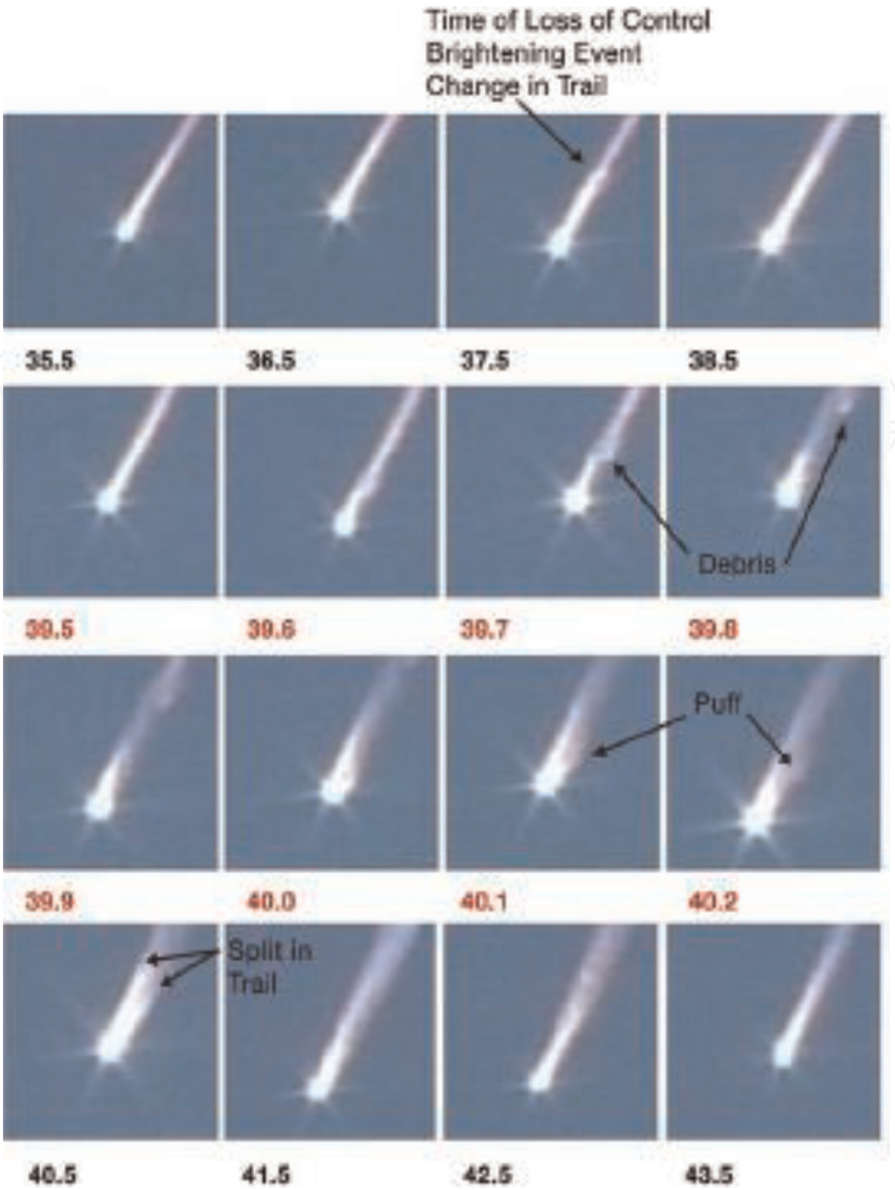

Figure 19.
Initiation phase of the destruction process (phase I) [25].

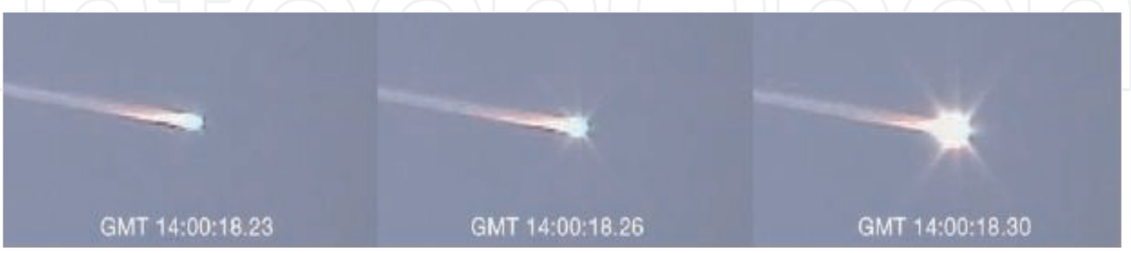

Figure 20.
Acceleration phase of the destruction process (phase A) [25].

It is known that satellite equipment is covered by a protection box which shields them against environmental factors such as cosmic radiation, solar wind, light (ultraviolet, visible, infrared), cosmic dust, and rarefied atmosphere. Usually, this box is a prism which has a pretty low dynamic drag, and, as a result, reaching high temperatures on the surface of the satellite is delayed; therefore the satellite disintegration is delayed during reentry. The situation is even more critical in the

Figure 21.
Total dispersal phase (phase D) [25].

case of the last stages of launching rockets which have a good aerodynamic shape in order to have a low aerodynamic drag during the ascending phase of the launch.

According to the space equipment design presented in this paper, special doors must be incorporated in the external fairing of the space equipment. The holes in the fairing can have any shape (rectangular, triangular, hexagonal, circular, etc.) depending on the position of the fairing. Doors fitted on every hole must be articulated by a cylindrical articulation (i.e., to permit a rotation of the door around an axis); this allows the door to open to the interior of the box when external pressure increases and to close when the pressure inside the fairing is higher than the external pressure. The door is fixed to the fairing through brazing with low fusible metals or strong resins (Loctite, Araldite) which decompose at low temperatures (150–200 to 700°C in special cases). Both the resin and metallic alloys must be extremely resistant at low temperatures but must lose their strength when temperature reaches several hundreds of degree Celsius. In in the early stages of the reentry, the epoxy resins decompose at temperatures between 150 and 200°C, and the braze alloys are melting when the local temperature reaches 200–700°C. As a result, the doors (covers) are pushed inside the fairing, and the external air enters inside where stagnates reach extremely high temperatures. The new external geometry of the space equipment leads to an increase of aerodynamic drag and converts kinetic energy into heat, which enhances the burning process.

By placing more doors on the fairing, no matter how the space equipment rotates during reentry, at least one door is opened by the dynamic pressure, and the rest of them are closed by the same dynamic pressure. Heating inside the fairing is maximum due to air stagnation, which leads to a rapid disintegration of the space equipment.

If the covers (doors) are not articulated, they are pushed inside the equipment by the ambient pressure acting on the surface of the fairing. Being pushed inside, the doors allow the air to flow inside the fairing around the equipment, but does not stagnate; thus heating does not occur, and the aerodynamic drag is low. For this reason the heating hate will be lower than when articulated covers are used.

For an even faster disintegration of the space equipment, the satellite components are wrapped in 0.05-mm thick aluminium or magnesium foil. These lightweight foils will burn first followed shortly by the equipment. This new technology can be seen in **Figures 22–27**.

Applying this design will determine the space debris to be disintegrated according to Space Shuttle Columbia's tragic disintegration phases I, A, and D.

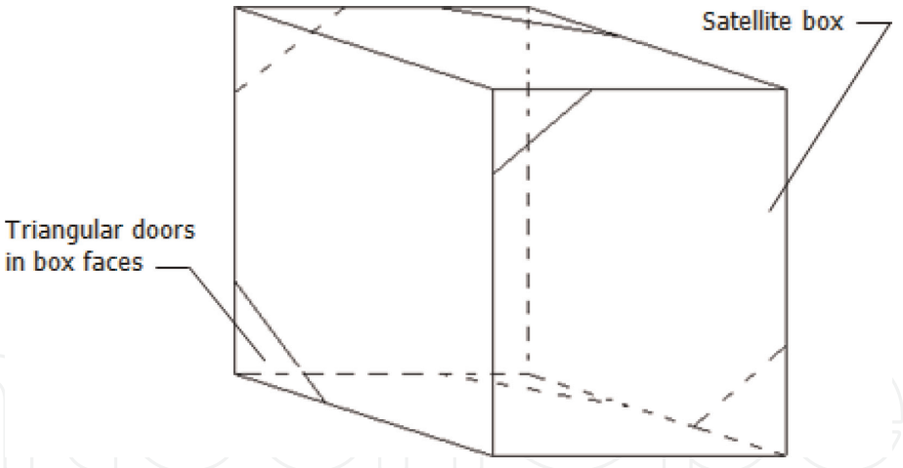

Figure 22.
Example of satellite box with doors.

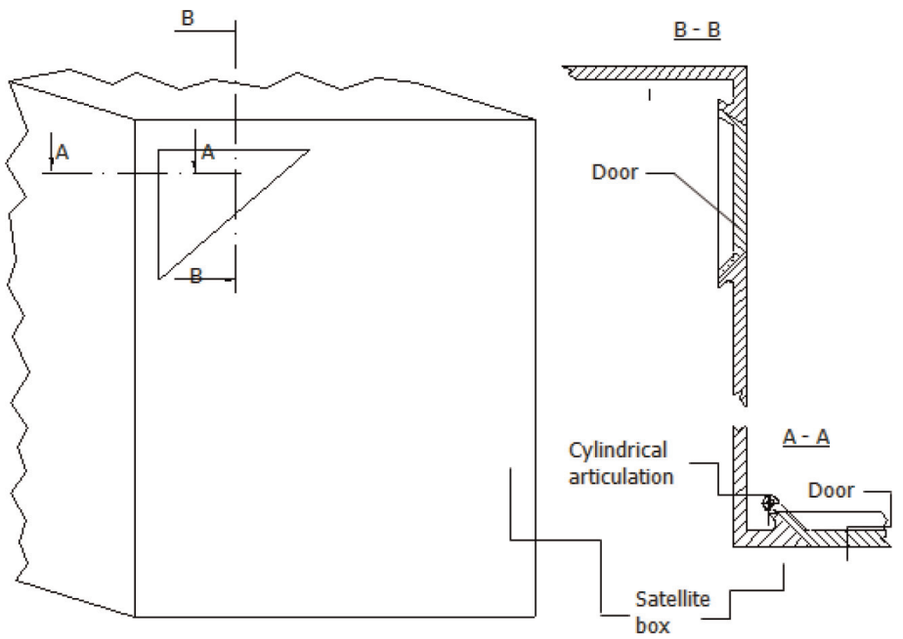

Figure 23.
Articulated door design.

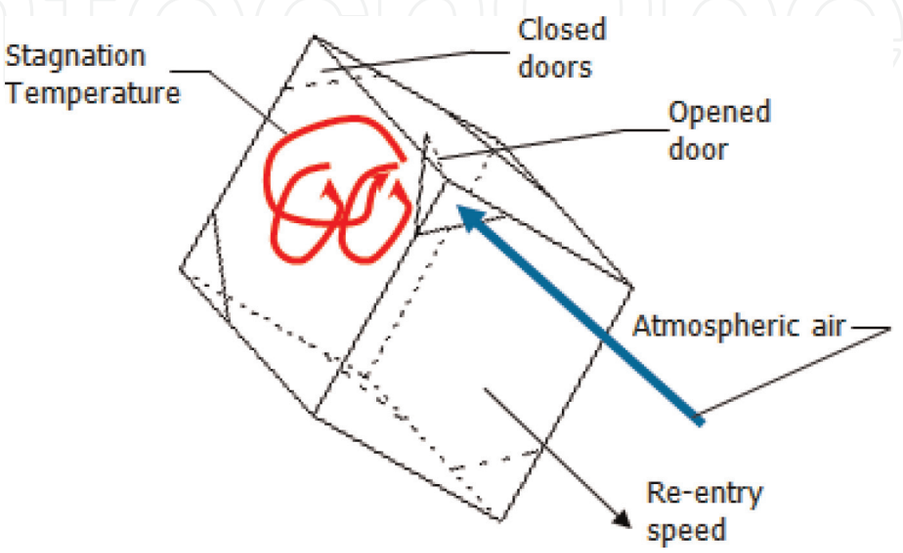

Figure 24.
Stagnation temperature inside the satellite box.

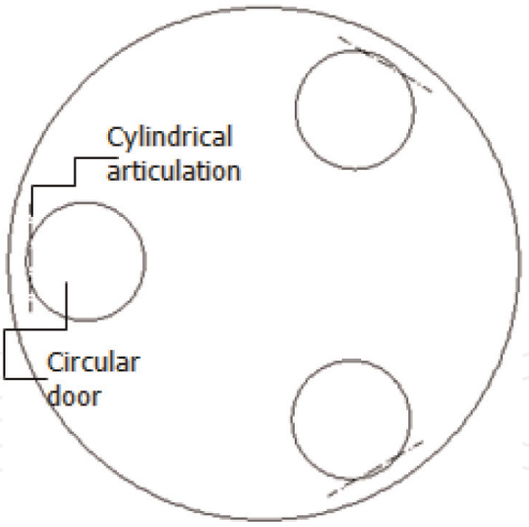

Figure 25.
Example of fuel tank with articulated circular doors.

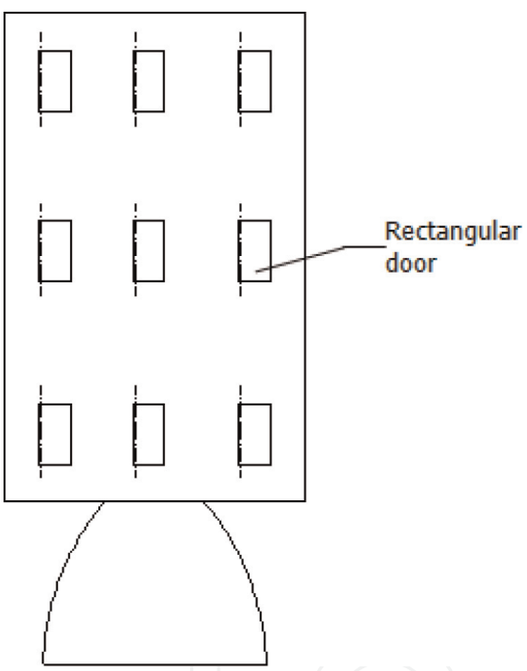

Figure 26.
Example of last-stage rocket with articulated rectangular doors.

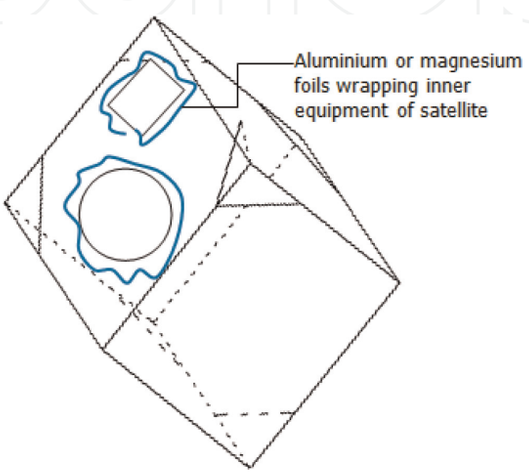

Figure 27.
Example of satellite equipment wrapped in aluminium or magnesium foil.

Author details

Constantin Sandu[1*], Cristian-Teodor Olariu[1] and Radu-Constantin Sandu[2]

1 Romanian Research and Development Institute for Gas Turbines-COMOTI, Bucharest, Romania

2 S.C. Structural Management Solutions S.R.L., Bucharest, Romania

*Address all correspondence to: constantin.sandu@comoti.ro

References

[1] Inside NASA's Plan to Catch an Asteroid. [Internet]. Available from: https://www.space.com/20612-nasa-asteroid-capture-mission-explained.html. [Accessed: 2019-05-29]

[2] Fifth European Conference on Space Debris. [Internet]. Available from: https://www.esa.int/About_Us/ESOC/Fifth_European_Conference_on_Space_Debris_to_address_key_issues. [Accessed: 2019-05-29]

[3] Ze Z. Space debris and present active debris removal techniques. In: Beijing Space Sustainability Conference; 13–14 October, 2011; Beijing; 2011

[4] Debris objects in low-Earth orbit (LEO). [Internet]. Available from: http://www.esa.int/spaceinimages/Images/2008/03/Debris_objects_in_low-Earth_orbit_LEO. [Accessed: 2019-05-29]

[5] Space Debris and Space Traffic Management. [Internet]. Available from: https://aerospace.org/article/space-debris-and-space-traffic-management. [Accessed: 2019-05-29]

[6] Alby F. Spot 1 end of life disposition maneuvers. Advances in Space Research. 2005;**35**:1335-1342

[7] SP1301-Position Paper-Space Debris Mitigation-Implementing Zero Debris Creation Zones. European Space Agency. [Internet]. Available from: http://www.esa.int/esapub/sp/sp1301/sp1301.pdf. [Accessed: 2019-05-29]

[8] Space Debris. [Internet]. Available from: http://www.esa.int/Our_Activities/Operations/Space_Debris/Mitigating_space_debris_generation. [Accessed: 2019-05-29]

[9] Solar Energy Fundamentals. [Internet]. Available from: http://physics.oregonstate.edu/~giebultt/COURSES/ph313/ppt/Ch06.1.pdf. [Accessed: 2019-05-29]

[10] Gold Coating. [Internet]. Available from: https://spinoff.nasa.gov/spinoff1997/hm2.html. [Accessed: 2019-05-29]

[11] The melting temperature of pure iron. [Internet]. Available from: https://www.chegg.com/homework-help/questions-and-answers/24-melting-temperature-pure-iron–1538-c-b-400-c-c-1147-c-d-727-c-25-eutectic-concentratio-q13180725. [Accessed: 2019-05-29]

[12] Robert P, Hoyt RP. An Architecture for Self-Fabricating Space Systems, AIAA SPACE 2013 Conference and Exposition; September 2013. DOI: 10.2514/6.2013-5509

[13] Electronic Imaging in Astronomy: Detectors and Instrumentation. McLean S. Springer Science & Business Media; 17 August, 2008. p. 86

[14] All-reflecting Two-mirror Telescopes. [Internet]. Available from: https://www.telescope-optics.net/two-mirror.html. [Accessed: 2019-05-29]

[15] Gregory James: Optica Promota; 1663. [Internet]. Available from: http://www.17centurymaths.com/contents/James%20Gregory/Definitions%20&%20Introductory%20Material.pdf. [Accessed: 2019-05-29]

[16] Geometry of a Sun-Synchronous Orbit. [Internet]. Available from: https://landsat.gsfc.nasa.gov/geometry-of-a-sun-synchronous-orbit/. [Accessed: 2019-05-29]

[17] Refractive Index for some common Liquids, Solids and Gases. [Internet]. Available from: https://www.engineeringtoolbox.com/refractive-index-d_1264.html. [Accessed: 2019-05-29]

[18] Tunable-focus liquid lens controlled using a servo motor. [Internet].

Available from: https://www.osapublishing.org/oe/fulltext.cfm?uri=oe-14-18-8031&id=97917. [Accessed: 2019-05-29]

[19] Aluminium- Specifications, Properties, Classifications and Classes. [Internet]. Available from: https://www.azom.com/article.aspx?ArticleID=2863. [Accessed: 2019-05-29]

[20] Phipps C, Birkan M, Bohn W, Eckel H-A, Hirosawa H, Lippert T, et al. Review: Laser ablation propulsion. Journal of Propulsion and Power. July-August, 2010;**26**(4)

[21] Brown MS, Arnold CB. Fundamentals of laser-material interaction and application to multiscale surface modification. In: Sugioka K et al., editors. Laser Precision Microfabrication. Springer Series in Materials Science. Vol. 135. Berlin, Heidelberg: Springer-Verlag; 2010, 2010. DOI: 10.1007/978-3-642-10523-4__4

[22] Ki H, Mohanty PS, Mazumder J. Modelling of high-density laser–material interaction using fast level set method. Journal of Physics D: Applied Physics. 2001;**34**:364-372

[23] Pakhomov A, Thompson MS, Swift W Jr, Gregory DA. Ablative laser propulsion: Specific impulse and thrust derived from force measurements. AIAA Journal. November, 2002;**40**(11): 2305-2311. DOI: 10.2514/2.1567

[24] Cause and Consequences of the Columbia Disaster. [Internet]. Available from: http://www.spacesafetymagazine.com/space-disasters/columbia-disaster/columbia-tragedy-repeated/. [Accessed: 2019-05-29]

[25] Columbia Crew Survival Investigation Report- NASA/SP-2008-565. [Internet]. Available from: https://www.nasa.gov/pdf/298870main_SP-2008-565.pdf. [Accessed: 2019-05-29]